

On the Offshore Advection of Boundary-Layer Structures and the Influence on Offshore Wind Conditions

Martin Dörenkämper · Michael Optis ·
Adam Monahan · Gerald Steinfeld

Received: 18 July 2014 / Accepted: 3 February 2015 / Published online: 24 February 2015
© Springer Science+Business Media Dordrecht 2015

Abstract The coastal discontinuity imposes strong signals to the atmospheric conditions over the sea that are important for wind-energy potential. Here, we provide a comprehensive investigation of the influence of the land–sea transition on wind conditions in the Baltic Sea using data from an offshore meteorological tower, data from a wind farm, and mesoscale model simulations. Results show a strong induced stable stratification when warm inland air flows over a colder sea. This stratification demonstrates a strong diurnal pattern and is most pronounced in spring when the land–sea temperature difference is greatest. The strength of the induced stratification is proportional to this parameter and inversely proportional to fetch. Extended periods of stable stratification lead to increased influence of inertial oscillations and increased frequency of low-level jets. Furthermore, heterogeneity in land-surface roughness along the coastline is found to produce pronounced horizontal streaks of reduced wind speeds that under stable stratification are advected several tens of kilometres over the sea. The intensity and length of the streaks dampen as atmospheric stability decreases. Increasing sea surface roughness leads to a deformation of these streaks with increasing fetch. Slight changes in wind direction shift the path of these advective streaks, which when passing through an offshore wind farm are found to produce large fluctuations in wind power. Implications of these coastline effects on the accurate modelling and forecasting of offshore wind conditions, as well as damage risk to the turbine, are discussed.

Keywords Coastal meteorology · Low-level jets · Offshore wind farms · Stable stratification · Wind energy

M. Dörenkämper (✉) · G. Steinfeld
ForWind - Center for Wind Energy Research, Institute of Physics, Carl von Ossietzky
University Oldenburg, Ammerländer Heerstr. 136, 26129 Oldenburg, Germany
e-mail: martin.doerkenkaemper@uni-oldenburg.de

M. Optis · A. Monahan
School of Earth and Ocean Sciences, University of Victoria, Victoria, BC, Canada

1 Introduction

1.1 Background

Offshore wind-energy capacity has grown considerably in the last decade: in 2013, 7.0 GW total offshore wind-energy capacity was connected to the grid globally, of which 93 % was installed in Europe (GWEC 2013). The European Wind Energy Association (EWEA) expects offshore wind energy in Europe to grow to 133 GW in the next few decades, with much of the added capacity to be located in the North and Baltic Seas. At present, two thirds of Europe's installed offshore wind capacity is located in the North Sea, followed by the Baltic Sea (17 %) and the Atlantic Ocean (16 %) (EWEA 2014). As there are so far only prototypes of floating turbines, today's offshore wind farms must be constructed close to the coastline where water depths are <50 m (EWEA 2013). Within this coastal region, complex flow regimes often develop due to the surface discontinuity at the coastline, across which large differences in surface roughness and temperature generally exist.

Unlike a purely offshore environment, the wind profile in the coastal region is generally not in equilibrium with the underlying sea surface. Consequently, various physical phenomena unique to the coastal region complicate the modelling and forecasting of wind conditions. The acceleration of the flow as it moves from land (high surface roughness) to sea (low roughness) is one well-known phenomenon, and can occur over fetches up to 70 km or more (Barthelmie et al. 2007). The deceleration of the flow occurs in the reverse direction.

In addition, the temperature differences between land and sea result in two general flow phenomena: the first is the sea breeze, involving cold-air advection from the sea towards the land, with the reverse process occurring at night. The other phenomenon is the induced stratification for flow from land to sea. When cold air flows over a warmer sea, induced unstable conditions develop and due to the enhanced buoyancy-driven turbulent mixing these unstable conditions persist only over a short fetch. Conversely, when warm air flows over a colder sea, an induced stable stratification develops, which due to the reduced turbulent mixing can persist for several hundred kilometres (Smedman et al. 1997). Furthermore, the reduced turbulent mixing results in the increased influence of inertial oscillations and thus the increased frequency of low-level jets (LLJs) in the coastal region (Smedman et al. 1996).

The importance of atmospheric conditions on power production from offshore wind turbines has been demonstrated previously. In their analytic wind-farm model, Emeis (2010) demonstrated the impact of atmospheric stability on the power deficit of large wind farms. On the scale of a single wind turbine, Dörenkämper et al. (2014) found differences in the power output of up to 15 % between stable and unstable stratification for wind turbines in free-flow conditions. Hansen et al. (2012) found that there is a near-linear relationship between the power deficit along a row of a wind farm and the turbulence intensity, with a decreased power deficit in a highly turbulent atmosphere.

The Baltic Sea is semi-enclosed, meaning that it is almost completely surrounded by land, and consequently the coastline discontinuity has a considerable influence on wind conditions over the Baltic Sea. In particular, stable stratification is frequent and strong, especially in spring when the surface temperature difference between land and sea can be 15–20 K or greater (Smedman et al. 1997). This is in contrast to the North Sea and the Atlantic Ocean that are not semi-enclosed. The atmospheric boundary layer in the coastal region over these seas tends to be neutrally or weakly unstably stratified (Sathe et al. 2011), albeit periods of stable stratifications do exist (Foreman et al. 2015).

Due to its unique features, the flow regime in the Baltic Sea has been the subject of considerable atmospheric research over the last several decades, with a particular emphasis

on offshore wind power. An extensive research campaign in the mid-1990s used a combination of aircraft measurements, onshore tower data, radiosoundings and numerical simulations to investigate the extent of the induced stratification and formation of LLJs in the Baltic Sea (e.g. Tjernström and Smedman 1993; Smedman et al. 1996, 1997). They found that in the sea region off the south-eastern Swedish coast stable conditions were present 66 % of the time over the Baltic Sea, and over half of these cases were described as *very stable* ($Ri > 0.25$, Ri being a bulk Richardson number) (Smedman et al. 1997). During an isolated period of very stable conditions, Smedman et al. (1996) found LLJs in 63 % of the wind profiles. In the comparatively rare event of unstable stratification, roll circulations were reported above the island of Gotland (Smedman 1991). Tjernström and Grisogono (1996) and Grisogono and Tjernström (1996) investigated a sea-breeze circulation in the south-eastern Swedish area that was found to be strongly related to the terrain geometry.

The evolution of the flow as warm air flows over cold water has been described by Csanady (1974) in terms of a quasi-equilibrium flow model: initially, a strong stable internal boundary layer (IBL) forms at the sea surface beneath a warm neutral upper layer. As fetch increases, the stable IBL increases with depth and near-surface stratification decreases. As the sea-surface temperature and near-surface air temperature reach equilibrium, a shallow neutral layer develops, and the stable IBL evolves into an elevated inversion between two neutral layers. Eventually the inversion reaches a quasi-equilibrium altitude and depth that can be maintained for considerable distances. Csanady (1974) analytically related the horizontal temperature gradient between the land and sea to both the time taken to reach equilibrium and the height of the inversion layer.

This quasi-equilibrium model has also been investigated in the Baltic Sea. Pryor and Barthelmie (1998) used data from a near-shore meteorological tower (2 km from coastline) and found that the flow is on average not in equilibrium with the sea surface. Smedman et al. (1997) used an idealized two-dimensional (2D) model to simulate the evolution of this quasi-equilibrium flow, which they found reached equilibrium after several hundred kilometres. Tjernström and Smedman (1993) investigated aircraft and tower measurements in the Baltic Sea along the south-eastern coast of Sweden in spring/early summer, and found that the quasi-equilibrium state is rarely achieved due to insufficient fetch. Lange et al. (2004) used tower measurements at Rødsand in the Baltic sea to propose a correction term to the logarithmic wind-speed profile in such cases where a stable IBL develops over the sea. Doran and Gryning (1987) worked with a network of onshore meteorological towers and offshore near-surface measurements, and found that the development of a shallow stable layer inhibits vertical momentum transfer.

1.2 Motivation and Intent of Study

The physical mechanisms controlling the coastal region wind regime are generally well understood and have been investigated and modelled successfully. However, these studies have been limited, in part due to the lack of high resolution offshore meteorological observations. Most of the observational studies in the Baltic Sea were largely constrained to onshore coastal meteorological towers and aircraft measurement campaigns with limited data (e.g. Tjernström and Smedman 1993; Smedman et al. 1996, 1997; Lange et al. 2004). Consequently, the ability to derive a detailed climatology of the coastal region wind regime, particularly in the Baltic Sea, has been lacking. With the recent availability of high resolution remote sensing and tall tower observations in the North and Baltic Seas, long-term climatological studies on the offshore wind conditions in these seas can now be conducted (e.g. Hasager et al. 2011; Peña et al. 2011).

Past studies have also been limited by the lack of high resolution mesoscale model simulations; early simulations were often limited to two dimensional (e.g. [Doran and Gryning 1987](#); [Lange et al. 2004](#)). Increasing computing resources allowed three-dimensional (3D) simulations; [Bergström \(2001\)](#) employed the MIUU model from Uppsala University in the Baltic Sea with a horizontal resolution of 9 km, and in the study of [Barthelmie et al. \(2007\)](#), a 5-km horizontal resolution mesoscale simulation was analyzed. Based on their results, they recommend more comprehensive modelling and data analysis of the offshore boundary layer. More recently, [Vincent et al. \(2013\)](#) conducted 2-km horizontal resolution 3D mesoscale simulations for the Baltic Sea to investigate spectral properties of the flow.

Although able to capture general features of the coastal flow regime, these 3D simulations lack sufficient resolution to resolve small-scale effects on the offshore flow deceleration, such as the influence of onshore isolated high roughness patches. The emergence of high resolution numerical models present an opportunity to investigate the coastal wind regime at a higher level of detail than in previous studies. A more robust analysis of the coastal flow regime is particularly relevant given the emergence of offshore wind farms in the coastal zone and the need for accurate wind resource assessments and forecasting.

The intent of this analysis is to investigate the character of the offshore coastal wind regime using more extensive datasets and higher resolution numerical simulations than previously. Altitudes relevant to wind-power production are of particular focus. A combination of offshore meteorological tower data, offshore wind-farm data and a high resolution mesoscale model are employed (described in Sect. 2). The study will specifically focus on: the climatology of induced stratification as well as its diurnal cycle; the strength of the stratification as it relates to fetch and land–sea temperature difference; the effect of induced stratification on wind shear; a climatology of LLJs; and the effect of spatially variable onshore roughness together with changing atmospheric stratification on fluctuations in wind speed and wind power.

Data sources used are described in Sect. 2, while results are presented in Sect. 3, followed by a discussion and conclusions in Sect. 4.

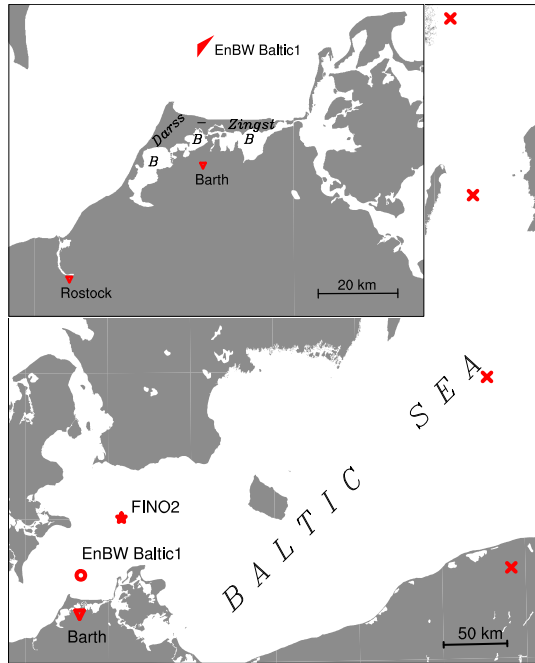
2 Data

2.1 FINO2 Tower Observations

The *Forschungsplattformen In Nord- und Ostsee* (FINO) project began in the early 2000s and now consists of three offshore research platforms in the North and Baltic Seas, all of which have 100-m meteorological towers. Meteorological parameters are recorded at frequencies of 1–10 Hz, and data are averaged in intervals ranging from 10 to 30 min.

For this study, a 6-year dataset of meteorological data (January 2008–December 2013) from the FINO2 mast in the central Western Baltic Sea (55.00°N 13.15°E; red star in Fig. 1) have been analyzed. This offshore meteorological mast was erected in 2007 and provides measurements of wind speed [Vector A100 cups (accuracy: $\pm 0.2 \text{ m s}^{-1}$) at heights of 32, 42, 52, 62, 72, 82, 92, 102 m above mean sea level], wind direction [Thies wind direction sensor ($\pm 1^\circ$)—31, 51, 71, 91 m], temperature/humidity [Thies hygro-thermo transmitter ($\pm 2\%$ relative humidity, $\pm 0.15 \text{ K}$)—30, 40, 50, 70, 99 m] and pressure [Vaisala PTB100A ($\pm 0.3 \text{ hPa}$)—30, 90 m] ([FINO2 2007](#)). Ten-minute averages from this dataset were available. Wind-speed measurement devices are mounted on the south-south-westerly side of the tower, and thus wind-speed measurements for north-north-easterly (specifically 350° – 040°) wind

Fig. 1 Map of the Western Baltic Sea. The *triangle* in the *upper panel* marks the position and extent of the wind farm “EnBW Baltic 1” (EB1), the “B” marks the position of the “Bodden” (lagoons), the *red crosses* in the *lower panel* mark data points used for the analysis in Sect. 3.1



directions are affected by the mast shadow. Wind-speed data for this direction range are excluded from the analysis.

2.2 Numerical Simulations

We employ the Weather Research and Forecasting model (WRF, Version 3.6.1) (Skamarock et al. 2008), consisting of three two-way nested domains [$\Delta_{x,y} = 18.9$ (D1), 6.3 (D2), 2.1 km (D3) spacing] in which an inner domain [$\Delta_{x,y} = 0.7$ km (D4)] is nested one-way (Fig. 2). The innermost domain covers the Darß-Zingst peninsula in the western Baltic Sea, with the wind farm “EnBW Baltic 1” (EB1) at about the centre of the domain. The position and extension of the EB1 wind farm is illustrated in Fig. 1 (upper panel). The model is initialized using the National Centers for Environmental Prediction (NCEP) coupled forecast system model version 2 (CFSv2) (reanalysis) data at 6-h intervals for the atmospheric variables (NCEP 2011) and the Operational Sea Surface Temperature and Sea Ice Analysis (OSTIA) dataset for the sea surface temperature (Donlon et al. 2012). Nudging of the horizontal wind vector, potential temperature and water vapour mixing ratio was applied in the D1–D3 domains above a height of about 2500 m. In the vertical direction the grid consisted of 62 model levels, of which about 20 levels were located in the lowest 1000 m and six levels below 120 m.

Longwave and shortwave radiation fluxes are based on the Rapid Radiative Transfer Model (RRTM) and Dudhia parametrization schemes, respectively. A cumulus (Betts–Miller–Janjic) scheme is used for the two outermost domains only. The Mellor–Yamada–Janjić turbulence parametrization scheme (TKE 1.5-order) is employed within the planetary boundary layer (PBL) (Mellor and Yamada 1982). This scheme has been proven to be the best choice in stably stratified situations from validation against meteorological tower data in the North Sea (Draxl et al. 2014). The model is initialized 3 days prior to each time period of interest to

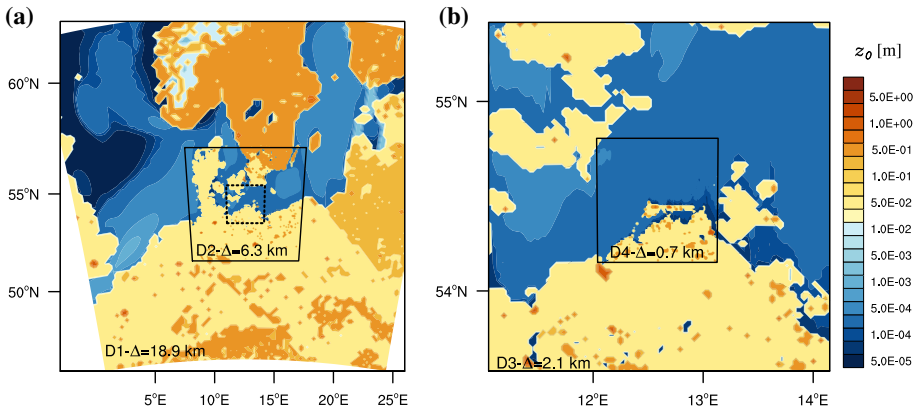


Fig. 2 Aerodynamic roughness length within the Weather Research and Forecasting (WRF) model for the two outermost domains (D1, D2) (a) as well as the innermost domains (D3, D4) (b). Note the differing horizontal resolution of the domains, indicated by the deltas in the lower left corners of the domains

allow for sufficient model spin-up time. A number of periods ranging from 48 to 120 h are investigated to cover a broad range of stratification, times of year and wind speeds.

2.3 Wind-Farm Data

About 16 km north of the Darß-Zingst peninsula an offshore wind farm (EB1), consisting of 21 Siemens SWT-2.3-93 wind turbines has been operating since May 2011. The wind turbines with a nominal power of 2.3 MW, a hub height of 67 m and a rotor diameter of 93 m are arranged in an irregular triangle [red triangle in Fig. 1 (upper panel)]. Power and wind data (10-min averages) from the Supervisory Control and Data Acquisition (SCADA) system of the wind farm are available and used within this study for model verification.

3 Results

3.1 Induced Stratification

We first examine the distribution of stratification (potential temperature difference between 99 and 30 m) at FINO2 by season. Defining stable stratification as conditions in which the potential temperature difference between 99 and 30 m (i.e. $\Delta\theta_{99-30}$) > 0.3 K (i.e. above the limit of accuracy for the temperature sensors), we find that stable stratification exists 46% of the time at FINO2. Maximum frequencies of occurrence are in spring [March, April and May (MAM); 77%] and summer [June, July and August (JJA); 51%] and minimum frequencies of occurrence are in autumn [September, October and November (SON); 27%] and winter [December, January and February (DJF); 27%]. This seasonal trend is illustrated in Fig. 3 through probability density functions (PDFs) of $\Delta\theta_{99-30}$. As seen, the PDFs for MAM and JJA show larger tails for very stable conditions, during which time the land–sea temperature difference is greatest.

As discussed in Sect. 1, the strength of the induced offshore stratification depends on the land–sea temperature difference as well as on the fetch. First we examine these effects by considering a representative case study from the WRF model simulations in which warm

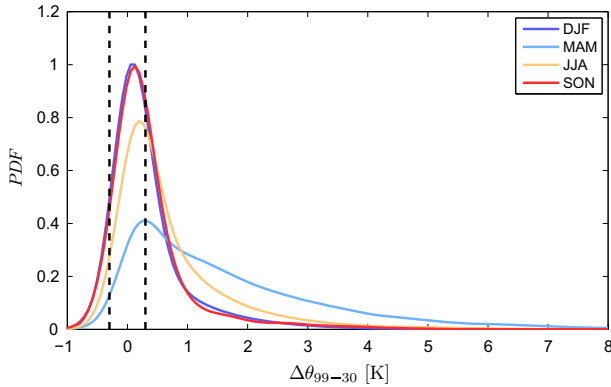
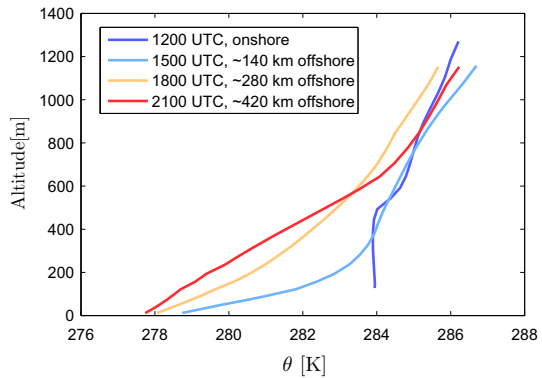


Fig. 3 Probability density function (PDF) of $\Delta\theta_{99-30}$ at FINO2, by season. Vertical dotted lines demarcate different stability regimes as defined in this analysis (i.e. unstable to the left, neutral between, and stable to the right)

Fig. 4 Potential temperature profile evolution on 10 April 2012 from the WRF simulation, beginning on land (1200 UTC) and captured upstream in 3-h increments (corresponding to roughly 140-km increments for the given wind conditions). The path begins off the north-east coast of Poland and crosses between the east coast of mainland Sweden and Gotland island



air flows from land to sea with relatively constant wind direction and with a fetch of at least several hundred kilometres. The flow on 10 April 2012 meets these criteria with a constant south-south-easterly wind throughout the day. Using the D1 WRF domain that encompasses most of the Baltic Sea, we track the flow beginning at the north-east coast of Poland heading north-north-west, passing between the east coast of mainland Sweden and the island of Gotland. Given the 3 h temporal resolution of the D1 simulation and a mean wind speed along this track of about 13 m s^{-1} , we can plot the evolution of the potential temperature profile at approximately 140-km intervals, beginning with an onshore profile. Fetch is limited to about 450 km for this case study, so only four time intervals spanning a total of 9 h can be considered. The corresponding locations are shown in Fig. 1 (lower panel) as red crosses.

The results of this analysis are shown in Fig. 4. The initial onshore potential temperature profile at 1200 UTC is approximately neutral below 600 m, capped by a distinct inversion. The atmospheric column becomes strongly stably stratified in the lower 200 m after 3 h in response to a land–sea temperature of about 6 K. After 6 h, the depth of the stable IBL increases considerably while the near-surface stratification reduces. After 9 h, the near-surface stratification has weakened further, and an elevated inversion layer between 200 and 600 m appears to develop, consistent with the quasi-equilibrium model (Csanady 1974). The fetch in

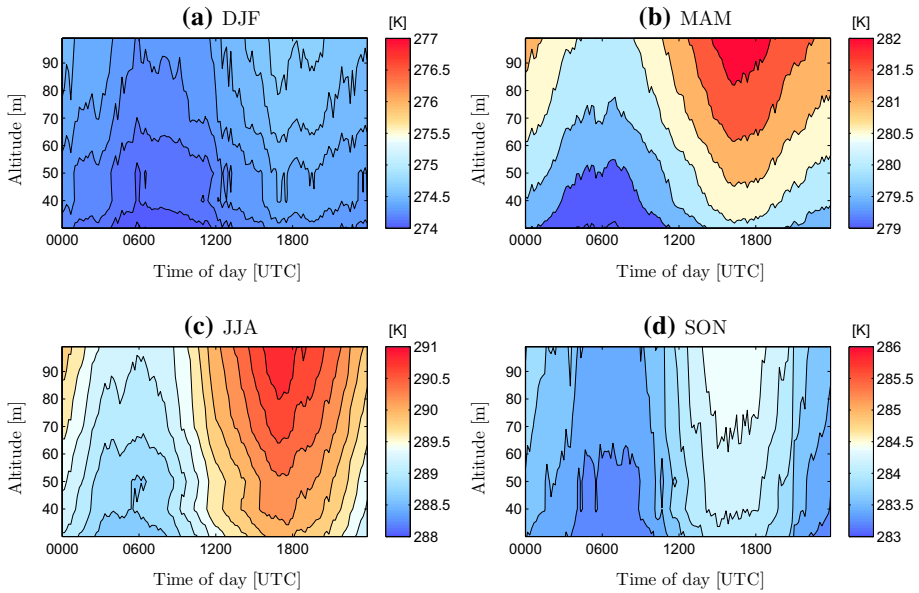


Fig. 5 Diurnal evolution of mean potential temperature by season at FINO2

this case study limits further development of the wind profile and thus the quasi-equilibrium state is not achieved.

Having demonstrated the role of fetch and land–sea temperature difference using the WRF model simulation, we now examine these effects in more detail using the observational data from FINO2. The effects of land–sea temperature difference and fetch are particularly pronounced at the FINO2 location. Surrounding land temperatures are usually higher in the southern Baltic Sea than in the northern part resulting in a greater land–sea temperature difference. The influence of land varies with wind direction since certain directions are associated with higher temperatures (e.g. warm weather from the south, cooler weather from the east). Fetch also varies considerably with wind direction, with limits of 40 km (e.g. north-westerly to northerly sector) and 575 km (e.g. north-easterly to easterly sector).

First, considering the seasonal influence on stratification, we examine the diurnal evolution of the mean potential temperature profile at FINO2 for the different seasons (Fig. 5). The atmosphere is on average stably stratified at all times and seasons, and shows a diurnal cycle with the highest temperatures and strongest stratification occurring at 1700 UTC. The strongest stratification and most pronounced diurnal cycles occur in spring and summer when the land–sea temperature difference is largest. Interpreting the diurnal cycle as an advective feature, the peak in the stable stratification in the evening is offset from the onshore peak in land-surface temperature by an advective time scale. Therefore, wind directions associated with low fetch are expected to have both stronger and earlier evening peaks in the stratification, with the opposite true for conditions of high fetch. This interpretation is consistent with the fact that the maxima and minima in Fig. 5 occur over a broad range of 1–3 h.

We examine this relationship between induced stratification and fetch in Fig. 6 using two measures of the induced stratification. The first is the mean potential temperature difference between 99 and 30 m during the evening peak in stratification (1400 UTC–2000 UTC, *evening* $\Delta\theta_{99-30}$ in Fig. 6). We refer to this as the *evening stratification* and note that this measure

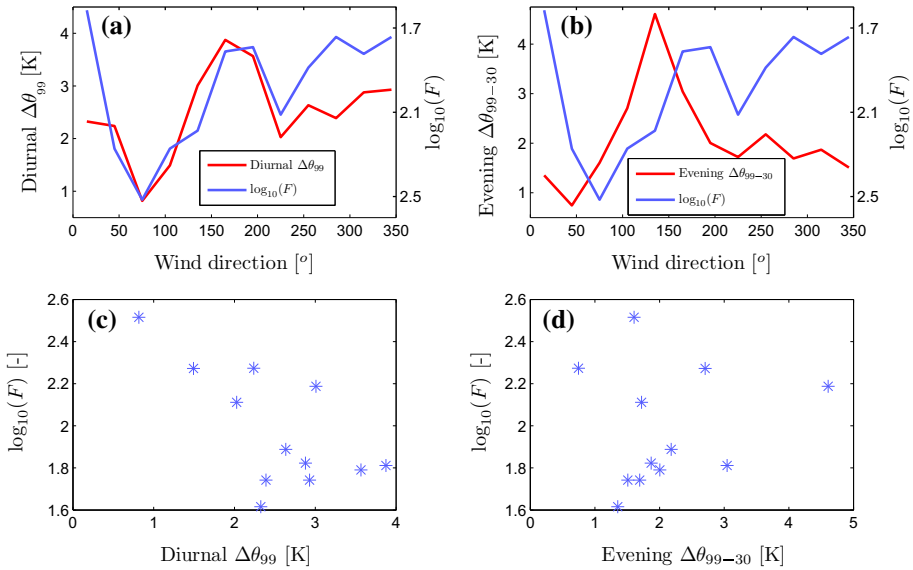
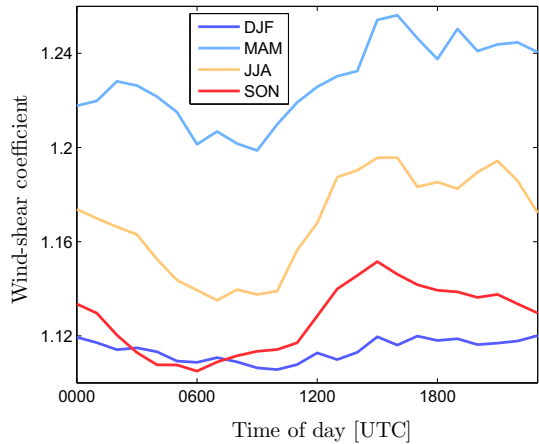


Fig. 6 Plots of **a** diurnal $\Delta\theta_{99}$ range and logarithm of upstream fetch (F) against wind direction, **b** evening stratification and logarithm of upstream fetch against wind direction, **c** logarithm of upstream fetch against the diurnal stratification, and **d** logarithm of upstream fetch against the evening stratification. Data at FINO2 for the MAM season only are used

will be biased towards wind directions associated with higher daily mean temperatures (e.g. southerly to south-westerly). The second measure is the difference between the mean 99-m potential temperature during the evening peak in stratification and the mean 99-m potential temperature during the morning minimum in stratification 0200 UTC–0800 UTC (*diurnal $\Delta\theta_{99}$* in Fig. 6). We refer to this measure as the *diurnal range*. This measure accounts mainly for the temperature difference due to land-surface heating/cooling and is less influenced by wind directions with higher daily mean temperatures. For this analysis, we consider only the spring season (when the diurnal cycle is greatest) and use wind-direction segments of 30°. Data are excluded if the mean 72-m wind direction in the morning differs by more than 30° from the mean 72-m wind direction in the evening, to ensure the flow direction is relatively constant throughout the day. This criterion excludes 65 % of the data.

In Fig. 6a, both the logarithm of upstream fetch and the mean diurnal stratification are plotted against wind direction. In Fig. 6c, the logarithm of upstream fetch for each wind direction segment is plotted against the mean diurnal stratification. In Fig. 6b and 6d, the same is plotted for the evening stratification. A strong relationship is evident between fetch and the diurnal stratification (Fig. 6a). In general, directions of low fetch (northerly, southerly and north-westerly sectors) are associated with the strongest degree of diurnal stratification, and directions of high fetch (e.g. north-easterly sector) are associated with the weakest diurnal stratification. The imperfect relation between these two measures (Fig. 6c), can be attributed to the relatively small sample size (552 days) in wind direction from the coastline to FINO2, and the large variability in fetch within a given 30° wind-direction segment. A much weaker relationship is evident between fetch and the evening stratification (Fig. 6b, d). In particular, weak stratification is observed for the northern sector despite low fetch, which is due to the lower daily mean temperature. Conversely, strong stratification is observed for the southern sector despite moderate fetch, which is due to higher daily mean temperatures.

Fig. 7 Wind-shear coefficient (ratio of 102-m and 32-m wind speeds) by season at FINO2, showing the mean coefficient by time of day



The induced stable stratification in the Baltic Sea has two main effects on the wind conditions: it increases near-surface wind shear and increases the frequency of LLJs. The former effect is illustrated in Fig. 7, in which the mean wind-shear coefficient (ratio of 102-m to 32-m wind speeds) at FINO2 is examined by season and time of day. The wind-shear coefficient is highest in spring when induced stratification is strongest. A distinct diurnal evolution is evident across all seasons but especially in spring and summer, with peaks in the wind-shear coefficient occurring between 1500 and 2200 UTC, which corresponds to the peaks in induced stratification (Fig. 5).

Extended periods of induced stratification result in increased frequency of LLJs at FINO2, which we explore in Figs. 8 and 9. We identify an LLJ event at FINO2 when wind speeds at any altitude below 102 m exceed the 102-m wind speeds by a specified percentage threshold, P_{LLJ} . Furthermore, we consider only cases in which 102-m wind speeds $> 3 \text{ m s}^{-1}$ (the cut-in speed for a typical offshore turbine). In Fig. 8a we consider a range of P_{LLJ} from 10–40% and plot the frequencies of occurrence of 10-min averaged LLJ events by season. Low-level jets are most frequent in spring when the induced stratification is strongest, and least frequent in winter when stratification is weakest. A histogram of LLJ occurrences by time of day is shown in Fig. 8b for MAM and JJA, with the criterion $P_{LLJ} = 20\%$ (DJF and SON are not considered due to insufficient amount of data). As seen in the figure, LLJ occurrences are relatively evenly distributed across all times of day in MAM due to the lower sea temperatures that can result in strongly stable stratification regardless of the time of day. Conversely, due to warmer seas in JJA, LLJ occurrences are slightly more frequent in late afternoon/early evening when air temperatures aloft are highest. The likelihood of an LLJ event at FINO2 is strongly dependent on stratification, as illustrated in Fig. 8c for MAM. In particular, there is about a 30% likelihood of an LLJ event when the potential temperature difference between 99 and 30 m exceeds 8 K. This relationship correlates to preferred wind directions for LLJ events (Fig. 8d) in MAM. In particular, the likelihood of LLJ events is largest in the southerly sector (11–12%) due to higher daily mean temperatures and low fetch. Conversely, LLJ events are less likely in the northerly sector (3–4%) despite low fetch due to the lower daily mean temperatures.

Extended periods of stable stratification can also lead to pronounced inertial oscillations at FINO2 (where the inertial period is roughly 17 h). Such events are common at nighttime in MAM and JJA when the air above both the land and sea is stably stratified for extended

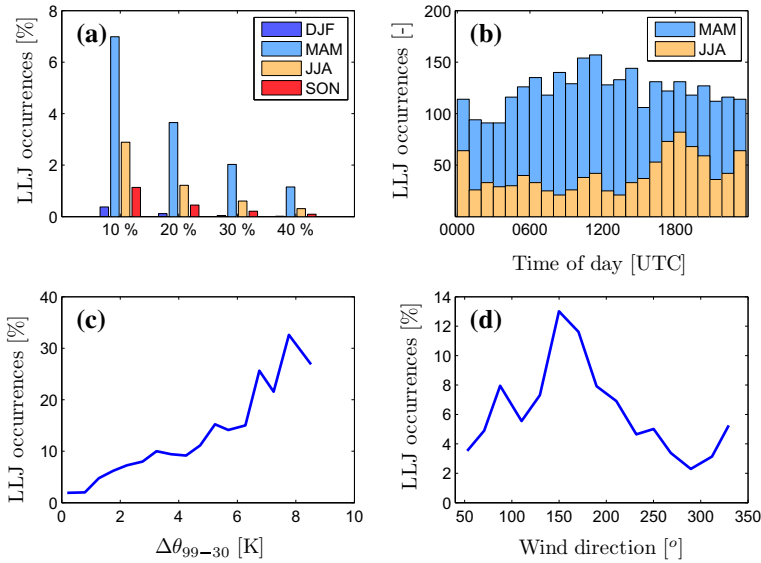


Fig. 8 Low-level jet (LLJ) climatology at FINO2, illustrating the occurrences of LLJs as they relate to **a** a season and P_{LLJ} (% increase in wind speeds at any altitude below 102 m, compared to wind speed at 102 m), **b** time of day (MAM and JJA only), **c** potential temperature difference between 99 and 30 m (MAM only), and **d** wind direction (MAM only)

periods. The large horizontal extent of stable stratification results in the development and evolution of the classic nocturnal LLJ. In Fig. 9, we demonstrate such an event beginning on 27 April 2008 at 1700 UTC and ending 17 h later. A plot of the time evolving 92-m wind vector is shown in Fig. 9a, demonstrating the well-developed inertial oscillation. Figure 9b shows the time evolution of $\Delta\theta_{99-30}$, which is strongest initially due to the advection of warm onshore air and maintains strong stable stratification throughout the event, providing sufficient conditions for the inertial oscillation. The oscillation results in cyclical behaviour of the wind profile (Fig. 9c). From 2300 UTC onward, the 92-m wind speed oscillates around the relatively constant 32-m wind speed. Figure 9d shows a contour plot of the wind-speed profile during the LLJ event. The most notable feature of the event is the rapid increase of wind speeds at upper altitudes up to 0000 UTC and decrease afterwards, which corresponds to an increase and then decrease in altitude of the LLJ.

3.2 Atmospheric Stability and Roughness Inhomogeneities

Within this subsection the near-coastal flow is studied in more detail using the WRF model as described in Sect. 2. From the simulated periods, 3 days with similar wind speed ($8\text{--}12\text{ m s}^{-1}$) and wind directions (southerly to westerly) but differing atmospheric stability have been chosen. Figure 10 shows 1-h averaged vertical profiles of wind speed, direction, squared Brunt-Väisälä frequency (N^2) and bulk Richardson number (Ri) within the PBL for the three selected days. The bulk Richardson number is defined as,

$$Ri = \frac{N^2}{(dU/dz)^2} \tag{1}$$

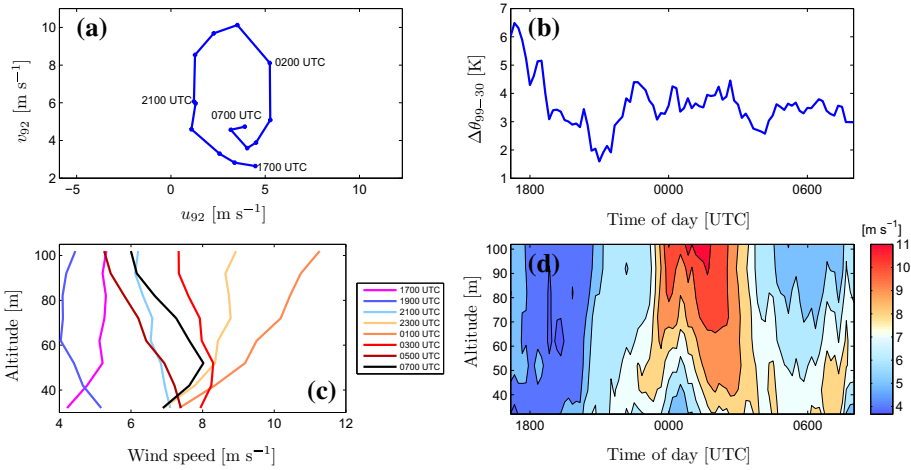


Fig. 9 Summary of a LLJ event on 27–28 April 2008, showing the **a** time evolution of the 92-m wind vector, **b** time evolution of $\Delta\theta$ between 99 and 30 m, **c** mean wind-speed profiles in 2-h intervals, and **d** contour plot of the time evolving vertical wind-speed profile

with U the horizontal wind speed and z the height above ground; N^2 is given by,

$$N^2 = \frac{g}{\Theta} \frac{d\Theta}{dz} \tag{2}$$

with g the acceleration due to gravity and Θ the potential temperature. Finite-difference approximations to the vertical derivative are computed between the model levels. Stable, neutral and unstable conditions correspond to positive, near-zero, and negative Ri and N^2 , respectively.

The profiles taken from the innermost domain (i.e. D4) of the WRF model simulations are shown in Fig. 10 for two different locations. The dashed profiles are for the location of the wind farm (54.61°N 12.65°E—red triangle in Fig. 1) and the solid profiles show the vertical structure of the PBL for an onshore location about 30km upstream of the wind farm on the continent (54.34°N 12.72°E—“Barth” in Fig. 1).

In Fig. 10, conditions with stable, neutral, and unstable conditions offshore are presented in the left, centre, and right columns respectively. The height of the PBL is around 800–1000m in all the situations. The largest difference between these situations can be observed in the Ri and N^2 values characterizing the stability.

3.2.1 Stable Stratification

In the situation with stable stratification (left column in Fig. 10; 23 July 2012), warm air from the continent is advected over the sea, leading to a development of a stable near-surface stratification. Over the land, the stratification changes from slightly stable during the morning hours to unstable around noon, returning to stable during the night. The potential-temperature difference ($\Delta\theta = \theta - \theta_0$) field interpolated to hub height ($z = 67$ m; EB1 wind farm) on the D4 domain is shown in Fig. 11a for 0600 UTC and Fig. 11b for 1200 UTC. As a reference temperature θ_0 , the temperature at hub height at the wind-farm location was chosen. The lowest temperatures over the sea occur at midday, and above land in the early morning. In general, the horizontal gradients in potential temperature are perpendicular to

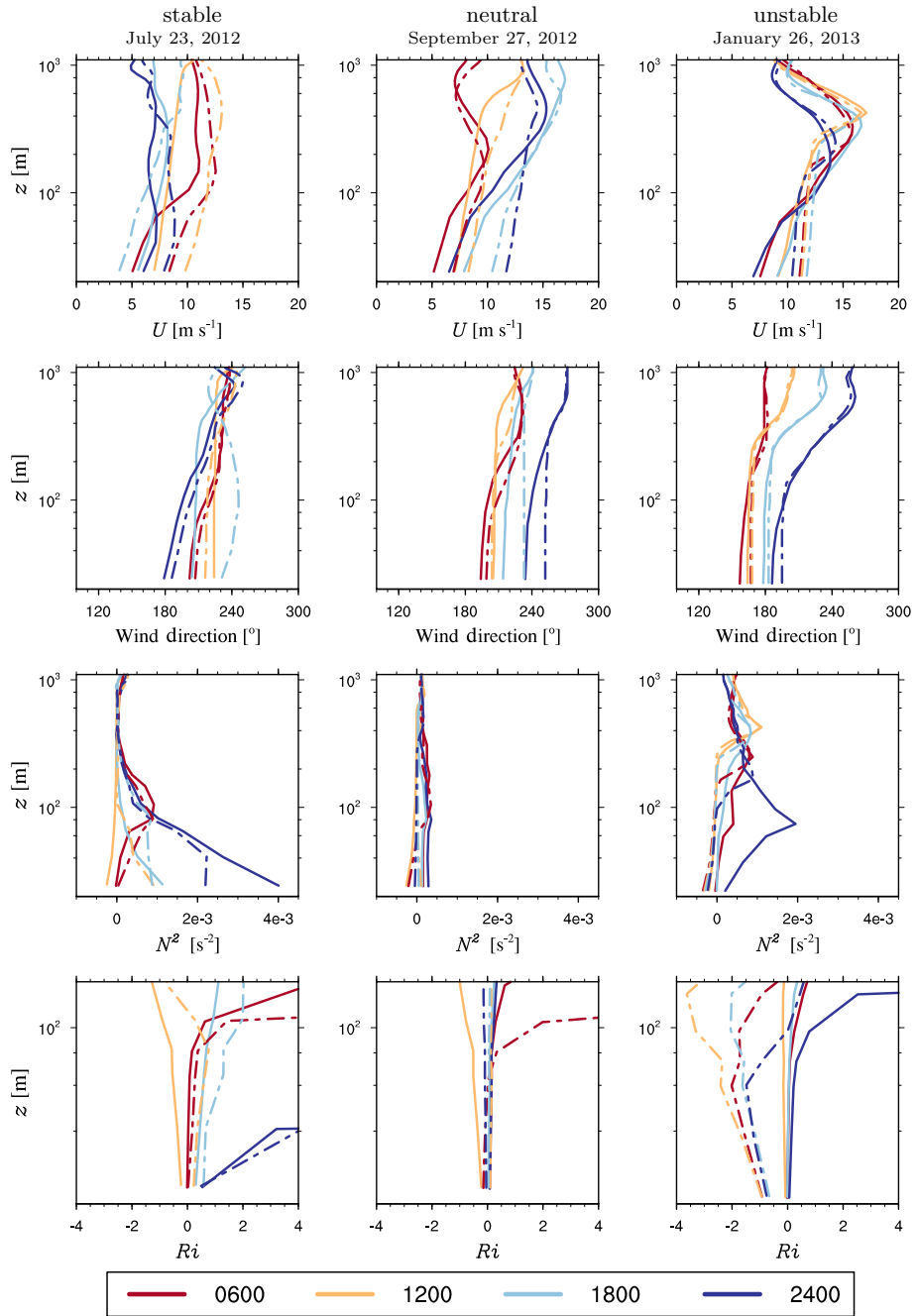


Fig. 10 Vertical profiles from WRF model simulations for different atmospheric stabilities [stable, neutral, unstable (*columns*)] at an onshore (*solid*) and an offshore (*dashed*) site. The stability class of the three cases was evaluated at the offshore site. The *top row* shows the wind speed, the *second row* the wind direction, the *third row* the squared Brunt–Väisälä frequency and the *lowest row* the bulk Richardson number for 0600 UTC (red), 1200 UTC (orange), 1800 UTC (light blue) and 2400 UTC (dark blue)

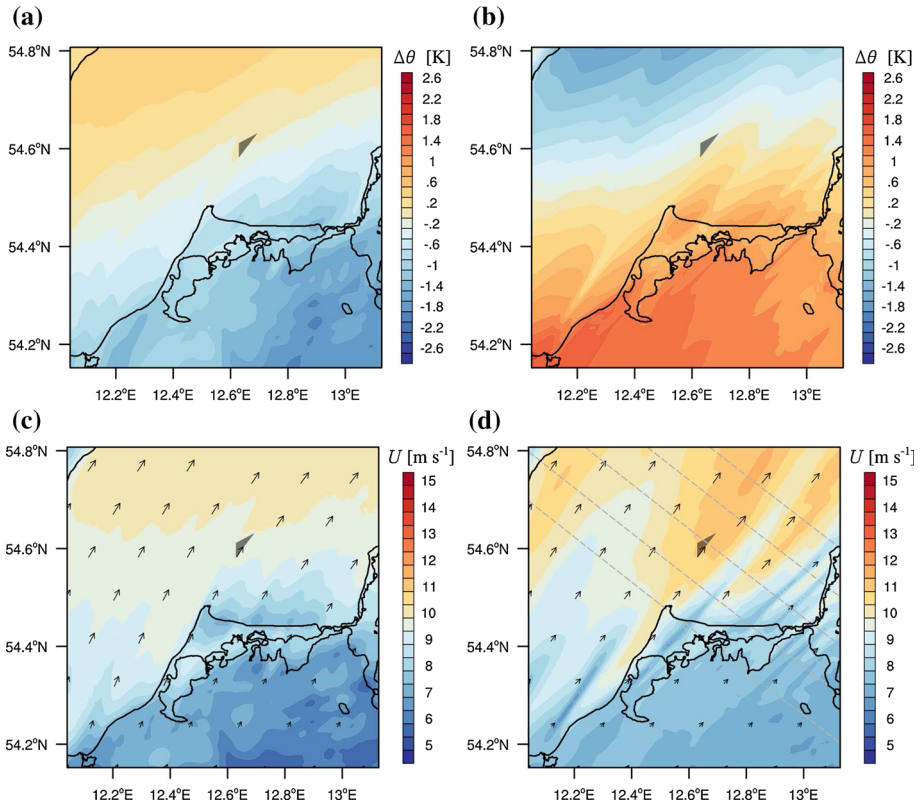


Fig. 11 Hub-height fields ($z = 67$ m) of potential temperature difference (a, b) and wind speed (c, d) obtained from WRF model simulations during stable offshore conditions on 23 July 2012 at 0600 UTC (left) and 1200 UTC (right) (hourly averages). The grey shaded triangle marks the position and extent of the wind farm. The grey dashed lines in d indicate the location of the cross-sections shown in Fig. 12a

the coastline, which is consistent with the expected offshore advection of air from the land. Figure 11c and d show the corresponding wind fields at the same altitude. Around midday (1200 UTC), at which time the land–sea surface temperature difference (and thus the induced stratification) is greatest, intense horizontal gradients within the wind field develop associated with low wind-speed streaks extending north-west away from the coast. On a scale of <5 km, crosswind differences of more than 3 m s^{-1} are found. These streaks are a result of the small-scale variability in onshore roughness within the region (Fig. 2b). Specifically, the region is dominated by grass-covered sand dunes [$z_0 \sim \mathcal{O}(10^{-2})$ m] with small areas of pine forests [$z_0 \sim \mathcal{O}(1)$ m]. A particularly intense streak is observed coming from the south-west edge of Fig. 11d due to the high roughness of the city of Rostock [$z_0 \sim \mathcal{O}(1)$ m] (see Fig. 1). Due to the induced stable stratification and reduced turbulent mixing, these roughness-induced streaks are able to extend several tens of kilometres into the central Baltic Sea.

To show the magnitude of this deviation in more detail, cross-sections through the wind field at hub height, orthogonal to the wind direction (at the wind-farm location) at various distances upwind and downwind from the wind farm, are presented in Fig. 12a. The grey dashed lines in Fig. 11d mark the exact positions where the cross-sections are extracted from the wind field at hub height. For an upstream distance of 10 km to the wind farm (light blue

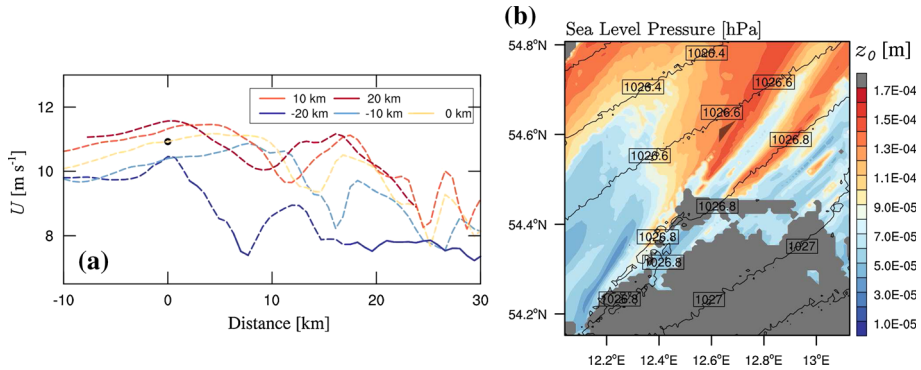


Fig. 12 Cross-sections of wind speed **a** orthogonal to the wind direction through the wind field at hub height at several distances away from the wind farm on 23 July 2012 at 1200 UTC. *Dashed lines* indicate that the underlying surface is water, *solid lines* indicate land. The *black circle* denotes the position of the wind farm EB1. Roughness length of the sea as well as surface pressure (*black lines*) are shown on the same day. The *grey shaded triangle* in **b** marks the position and extent of the wind farm

line in Fig. 12a), the minimum wind speed within the streak is located about 15 km south-east of the wind farm (0 km, black circle in Fig. 12a). With increasing downstream distance to the wind farm, the minimum is deflected towards the west by around 2.5 km per 10 km downstream distance. This deflection of the wind streaks can be explained by the horizontal pressure gradient driving the flow, together with a growing roughness length of the sea surface with increasing fetch. This relationship is shown in Fig. 12b. The roughness length in the central Baltic Sea is about twice as high as at the coastline. The gradient in z_0 also explains the increasing turning of the wind direction with decreasing height (not shown here). The reverse process occurs immediately at the coast, where a step change of the roughness by several orders of magnitude can be found. This is indicated in the second streak south-west of the wind farm (in Fig. 11d), which first turns slightly right and afterwards, with increasing coastal distance, left. In addition the long streak above the lagoon (the Bodden) south of the peninsula shows a deflection towards the right when entering the high surface roughness of the peninsula. It is also evident from Fig. 12a that the reduced wind-speed streaks weaken with increasing distance from the coastline. In particular, over a distance of 30 km [10 km upstream (light blue) to +20 km downstream (dark red)] an increase in the wind speed by 2 m s^{-1} within the streak can be found.

Figure 13a shows an along-wind vertical cross-section of the wind speed and N^2 within the PBL through the wind-farm location (0 km on the x -axis), along with the corresponding roughness length (bottom) averaged over 1 h. This cross-section is aligned parallel with the wind at EB1 and thus also roughly parallel to the coastline of the Darß-Zingst peninsula through the low wind-speed streak in the south-western edge of the domain (see Fig. 11d). Note that the wind direction does not change significantly within the PBL (Fig. 10). As the low-level air flows across the coastline, a stable stratification develops and increases in intensity over the first 15 km. With the reduced surface roughness over the sea, the flow accelerates and achieves equilibrium in the lowest 400 m after a fetch of about 70 km. Beyond this point, only a slight increase in the wind speed is found.

As shown in Fig. 10, the large-scale wind direction veers from southerly to south-westerly between the morning and the evening hours. This change in wind direction shifts the orientation of the low wind-speed streaks, which pass through the wind farm. This transition results in substantial fluctuations in wind speed and wind power at the wind-farm location.

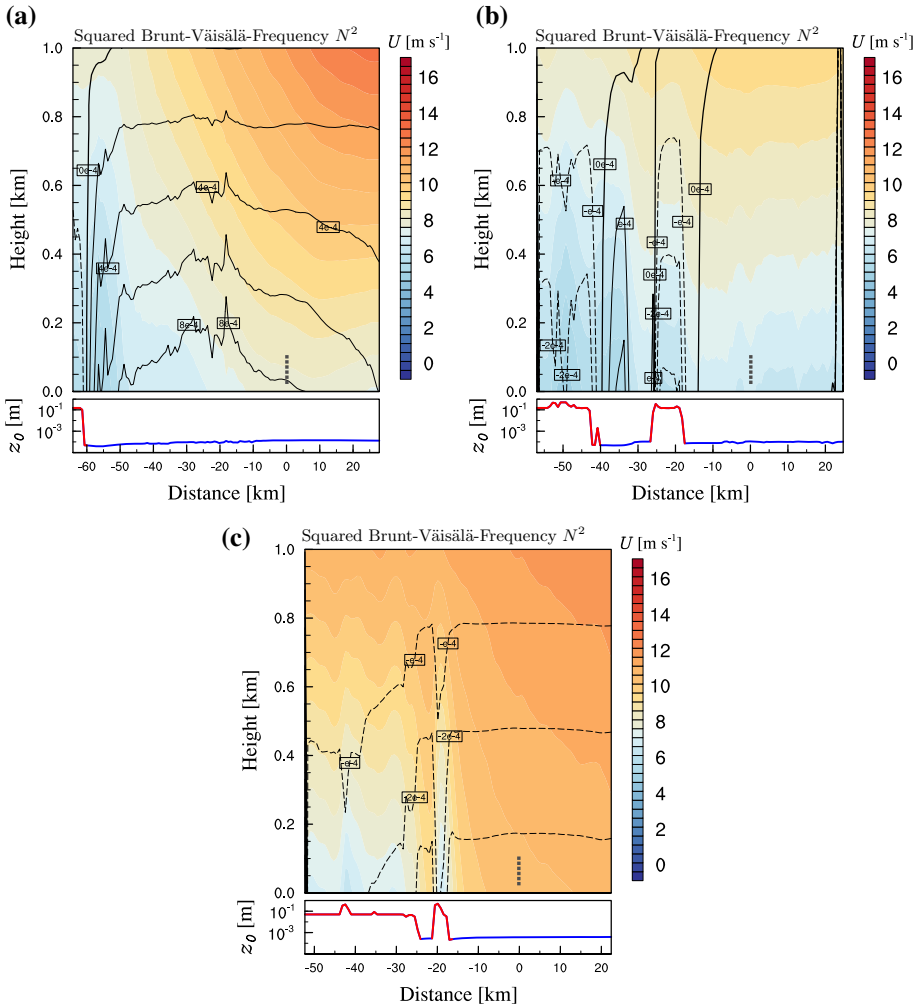


Fig. 13 Along-wind vertical cross-sections of wind speed (1-h averages) obtained from WRF model simulations during stable (a 23 July 2012—1200 UTC), neutral (b 27 September 2012—1200 UTC) and unstable (c 26 January 2013—1200 UTC) stratification and the corresponding underlying roughness length (bottom). Red lines in the roughness-length panel indicate that land is underlying, blue lines water. The black lines indicate isolines of $N^2[\text{s}^{-2}]$: positive values (stable) are solid, negative values (unstable) are dashed, the neutral isoline is bold. The position and vertical extent of the wind farm is marked with the bold grey dotted line in the upper panels

In Fig. 14, both the measured power from the windward turbine at the wind farm and the simulated wind power from the WRF model simulation are plotted over the course of the day. Also plotted are the measured and simulated wind direction. The simulated wind power was calculated according to,

$$P_{wind} = \frac{1}{2} \rho U^3 A, \tag{3}$$

where A is the rotor area, U is the horizontal wind speed and ρ is the density of the air (both obtained from the simulations). The measured wind power was scaled with the corresponding

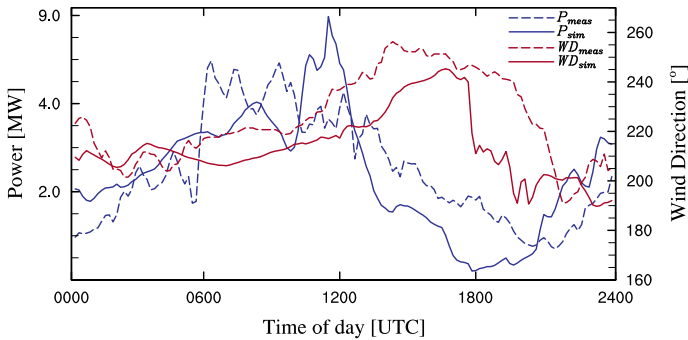


Fig. 14 Measured (*dashed*) and simulated (*solid*) wind power as well as wind direction on 23 July 2012 for a single wind turbine in free flow

power coefficient $c_p(U)$ of the wind turbine (from manufacturer specifications) to avoid the constant power above the turbine's rated wind speed. The figure indicates that the wind direction is modelled well by the simulation, albeit it is shifted in time slightly. The wind power shows strong fluctuations in the observed case from about 0600 UTC in the morning until noon. An increase in the simulated power fluctuation can be found around 1000 UTC. These strong fluctuations correspond to a slow veering of the wind towards the south-west and begin as soon as the wind direction is larger than 210° . The fluctuations are attributed to two factors: first, the advection of the wind-speed streaks to the wind-farm location and second, the shape of the coastline. For a south-westerly wind ($>210^\circ$) the sea fetch suddenly increases from about 15 km to more than 50 km [see Fig. 1 (upper panel)], resulting in a sudden increase in the wind speed as well. Note that the measured power fluctuates more than the simulated. This is most likely due to the limited horizontal resolution of the model of 0.7 km that is incapable of resolving all of the surface changes at the Darß-Zingst coast. This comparison of simulated and measured wind speeds underlines the importance of correct wind-direction forecasts in regions with complex coastlines.

A comparison of different PBL schemes for this stably stratified situation can be found in the Appendix.

3.2.2 Neutral Stratification

In the neutrally-stratified situation (Fig. 10—central column) in early autumn (27 September 2012) the wind speeds increase from around 8 to 12 m s^{-1} over the course of the day, while the wind direction at hub height veers between 200° and 260° . The wind direction is constant with height within the lowest 400 m at the offshore location. The PBL is near neutrally stratified throughout the day at the offshore location, while slight deviations from the neutral state develop onshore with the change of the radiative fluxes across the day (see Fig. 13b).

The hub-height fields of potential temperature difference (Fig. 15a, b) show the homogeneity in temperature, especially in the morning hours, where the overall difference across the domain is only about 1 K. The wind fields (Fig. 15c, d) are more homogeneous compared to the stable case. Streaks induced by the roughness length variations are still detectable but less pronounced in intensity because of the more turbulent PBL and the related mixing.

In the along-wind vertical cross-section at noon (Fig. 13b), a slightly unstable stratification can be found above land. Due to the differing wind direction (now 195° compared to 220° in the stable case), two land patches are crossed by the flow before moving above the Baltic Sea,

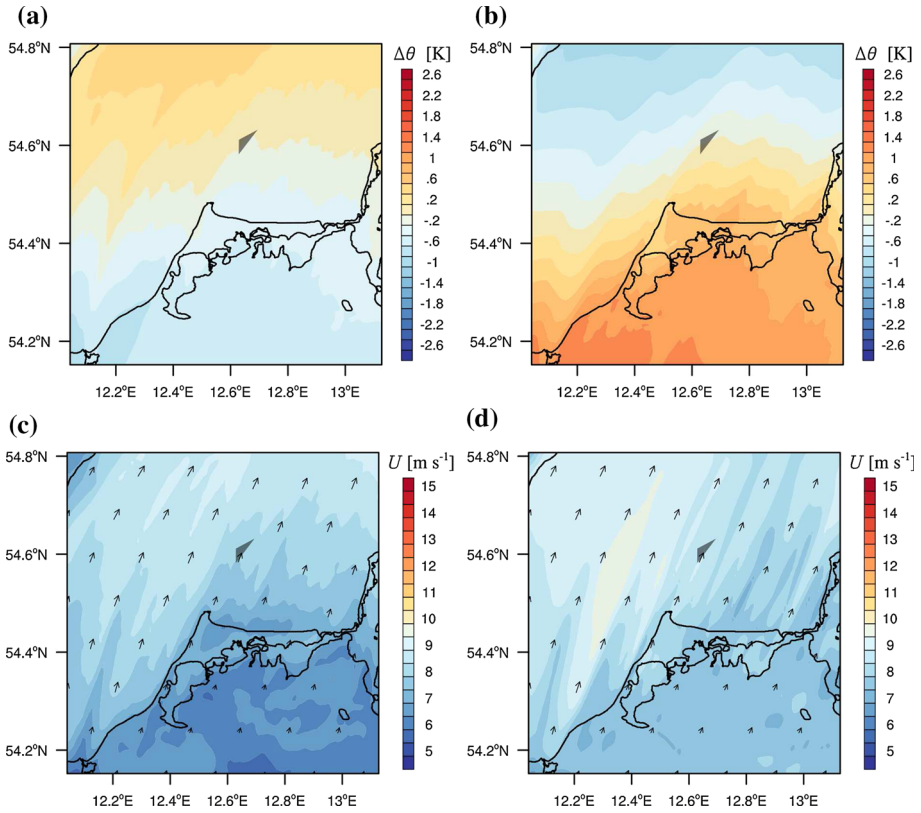


Fig. 15 Hub-height fields ($z = 67$ m) of potential temperature difference (a, b) and wind speed (c, d) obtained from WRF model simulations during neutral offshore conditions on 27 September 2012 at 0600 UTC (left) and 1200 UTC (right) (hourly averages). The grey shaded triangle marks the position and extent of the wind farm

separated by the Bodden (“B” in Fig. 1). The increased friction due to these patches of high roughness leads to a reduced wind speed in the boundary layer, compared to the situation above the sea. In addition, the differing surface temperatures induce a slight inhomogeneity in stratification. The flow starts unstably stratified above the continent, crosses the Bodden at about 40 km upstream distance to the wind farm, and develops a slightly stably stratified state. When the Darß-Zingst peninsula is crossed (25 km) an unstable stratification develops. Above the Baltic Sea the neutrally-stratified state develops after about 5 km and thus more rapidly than in the stable case. The wind shear is also less above the sea compared to onshore mainly due to the reduced surface roughness offshore.

3.2.3 Unstable Stratification

Hub-height horizontal fields for an unstably stratified situation in mid winter (26 January 2013—right column in Fig. 10) are presented in Fig. 16. Here, the lowest temperatures throughout the day are found onshore. The flow is from a south-south-easterly direction, veering to south over the day. The stratification is slightly unstable within the lowest 300 m during all of the day above the wind farm (Fig. 10). Above the land, a stable stratification

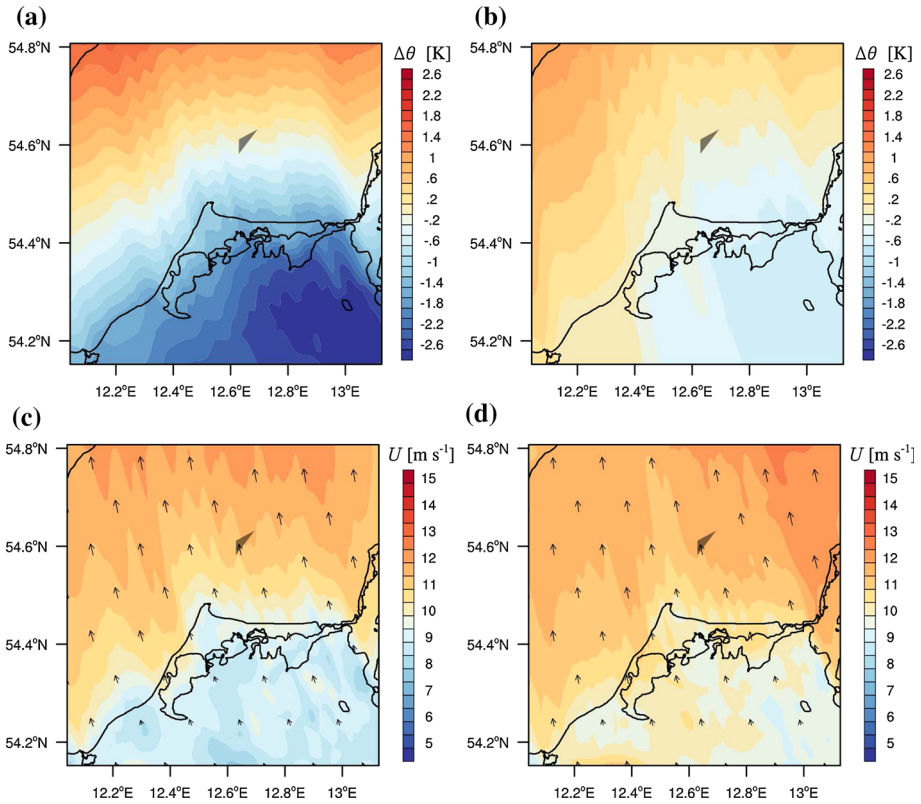


Fig. 16 Hub-height fields ($z = 67$ m) of potential-temperature difference (**a, b**) and wind speed (**c, d**) obtained from WRF model simulations during unstable offshore conditions on 26 January 2013 at 0600 UTC (*left*) and 1200 UTC (*right*) (hourly averages). The *grey shaded triangle* marks the position and extent of the wind farm

develops at night, while a neutral stratification is observed during the day. In the hub-height wind fields (Fig. 16c, d), the streaks as observed in the stable and neutral situations do no longer occur. The wind-speed gradients are generally low and are aligned with the coastline. At a distance of about 20 km from the coast, where the wind farm EB1 is located, the wind speed has already increased to the mean conditions of the central Baltic Sea (around 11 m s^{-1}) due to enhanced turbulent mixing.

The corresponding along-wind cross-section at noon (Fig. 13c) shows the development of a slightly unstable stratification ($N^2 = 0.0004 \text{ s}^{-2}$) when the flow crosses the warm water. Increased mixing due to the turbulence induced by the unstable stratification leads to the development of nearly constant wind speeds within the lowest 200 m. The wind-speed deficit that is induced by the underlying roughness propagates only a short distance into the central Baltic Sea due to this increased mixing.

4 Discussion and Conclusions

Our analysis demonstrates the importance of the land–sea temperature difference and onshore surface roughness in influencing the wind and stability conditions in the offshore coastal

area, and in particular the impact on the power output of offshore wind farms. A combination of long-term meteorological tower data, wind-farm data and high resolution mesoscale modelling data were used in this analysis, from which the following conclusions are deduced.

Observations using six years of data from FINO2 demonstrated that stable stratification predominates in the spring season, occurring in 77 % of the time. The stratification showed a pronounced diurnal cycle, which was strongest in spring and summer. The stratification peaked in late afternoon and was offset to the peak in land-surface heating by the expected advection time between the coastline and FINO2. A comparison of fetch to this diurnally induced stratification showed a strong inverse relationship. Strong stratification was particularly associated with southerly flow, due to higher daily mean temperatures typical of that sector. A WRF model case study of a constant wind direction and a long fetch showed the evolution of the potential temperature profile consistent with [Csanady \(1974\)](#). The quasi-equilibrium state was not fully achieved due to insufficient fetch, a result that is consistent with previous studies and is a general feature of the Baltic Sea, where fetch rarely exceeds several hundred kilometres. However, the case study selected had relatively high wind speeds (about 13 m s^{-1} at 72 m), which limited the development of the quasi-equilibrium state. A lower wind-speed case study would likely show significantly extended development, and would be a useful investigation in future studies.

Stable stratification at FINO2 was shown to have a large effect on the character of the wind profile. In particular, high wind shear was observed in late afternoon, corresponding with the peak in stable stratification. Furthermore, wind shear increased substantially in spring and summer when stable stratification was strongest. Further analysis of the FINO2 dataset showed the increased frequency of LLJs and the associated influence of inertial oscillations under extended periods of very stable stratification. LLJ events were evenly distributed throughout the day and occurred frequently at low altitudes (i.e. below 102 m). A case study of a full oscillation of the wind vector at FINO2 illustrated strong variability in the wind profile, which at some times decreased monotonically with altitude. A single case study was highlighted here, and a more comprehensive climatology of wind-profile variability due to the inertial oscillation would be useful in future studies.

These features of offshore LLJs at FINO2 are in sharp contrast to those of onshore LLJs, which are generally restricted to nighttime since this is generally the only extended period of stable stratification ([Baas et al. 2009](#)). Furthermore, onshore LLJs generally develop in heights of 150–300 m and rarely below 100 m ([Baas et al. 2009](#)), and onshore inertial oscillations are generally limited to <12 h of development (i.e. sunset to sunrise), which in mid-latitudes is less than a full inertial cycle.

Results from the high resolution WRF model simulations showed strong differences between offshore-oriented flow regimes under different stratifications. The most striking features under stable and neutral conditions offshore were intense streaks of reduced wind speeds induced by the underlying surface roughness that were advected several tens of kilometres over the sea. These features were absent in unstable conditions due to enhanced vertical mixing. In the vertical direction, a quasi-equilibrium was not achieved after 100 km fetch in stable stratification. Conversely, quasi-equilibrium was achieved in unstable conditions after <20 km of fetch, as the flow quickly adapted to the surface roughness change under increased mixing. The increasing roughness length of the sea surface with increasing fetch led to a veering of these streaks under stable stratification.

In stable conditions, slight changes in the wind direction of single degrees shifted the path of the advected low wind-speed streaks, which when passing through a wind-farm location led to substantial power fluctuations in time of the windward turbine. These variations were

found for both measured wind power as well as the simulated WRF case. This phenomenon highlights the need for precise forecasts of the wind direction in regions where complex coastlines are predominant, as slight changes to the fetch can lead to strongly differing horizontal wind-speed gradients for a given region. Fine horizontal resolution is required to capture these narrow features of the flow, as well.

The near-coastal streaks were not dependent on the PBL scheme (Appendix). A comparison of the results from the two innermost domains showed that the 2.1-km horizontal resolution domain (D3) is capable of resolving the general flow features close to the shore even though a more detailed distribution of the streaks was found in the higher resolution D4 domains.

The results demonstrate the need of long-term climatological measurements for the accurate assessment of the wind and stability conditions in the coastal area, where most projected offshore wind farms are located. We found that an extensive and high resolution modelling of the coastal wind conditions is needed not only for the long-term power estimation but also for operational wind-power forecasting, due to the impact of small-scale structures at the coastal discontinuity on wind and power fluctuations. These fluctuations in space and time not only pose a threat to electricity grid stability but also introduce fatigue risk to the turbines. In future studies comparison of mesoscale simulations with lidar data as well as satellite data could help to achieve additional insight into features of coastal winds.

Acknowledgments The work presented in this study is funded by the National Research Project Baltic 1 (FKZ0325215A, Federal Ministry for Environment, Nature Conservation and Nuclear Safety) and the Ministry for Education, Science and Culture of Lower Saxony. The DAAD is thanked for granting Martin Dörenkämper a 2-month stay at the University of Victoria, Victoria, BC, Canada. Adam Monahan and Michael Optis acknowledge the support of the Natural Science and Engineering Research Council of Canada through the Discovery Grant Program and the CREATE Training Program in Interdisciplinary Climates Science. The authors thank the Project Management Jülich (PTJ) and the Federal Maritime And Hydrographic Agency (BSH) for providing access to the data of the offshore research platform FINO2. The authors thank Yuko Takeyama for discussions on wind-speed streaks in coastal areas. The authors are grateful to Sonja Drüke, Robert Günther and Stefan Albensoeder for their help in setting up the WRF model.

Appendix: On the Influence of the PBL Scheme on Wind Conditions in Stable Stratification

To investigate the influence of the PBL scheme on the streaks described in Sect. 3.2.1, the simulations for 23 July 2012 were repeated with four different PBL schemes. Figure 17 shows hub-height fields of wind speed as in Fig. 11d obtained from the WRF model for four different PBL schemes: Mellor–Yamada–Nakanishi–Niino (MYNN) (a) (Nakanishi and Niino 2004), Yonsei-University (YSU) (c) (Hong et al. 2006) and Asymmetric Convective Model version 2 (ACM) (d) (Pleim 2007). In addition we also implemented a recent suggested modification of the Mellor–Yamada–Janjić (MYJv2) scheme (Foreman and Emeis 2012) for more accurate wind-energy forecasts into the WRF model (b). All other parametrization schemes were defined as described in Sect. 2.2.

The results show that streaks are detectable in all of the PBL schemes chosen. The intensity of the streaks is stronger and the length of the streaks greater with the YSU and ACM parametrizations and slightly weaker in the MYNN and MYJv2 schemes. Location and origin of the streaks (patches of high roughness on the Darß-Zingst peninsula) are the same for all parametrizations chosen. The wind field simulated with the MYNN (Fig. 17a) scheme shows a stronger deflection of the flow towards the right at the coastal passage and a weak-

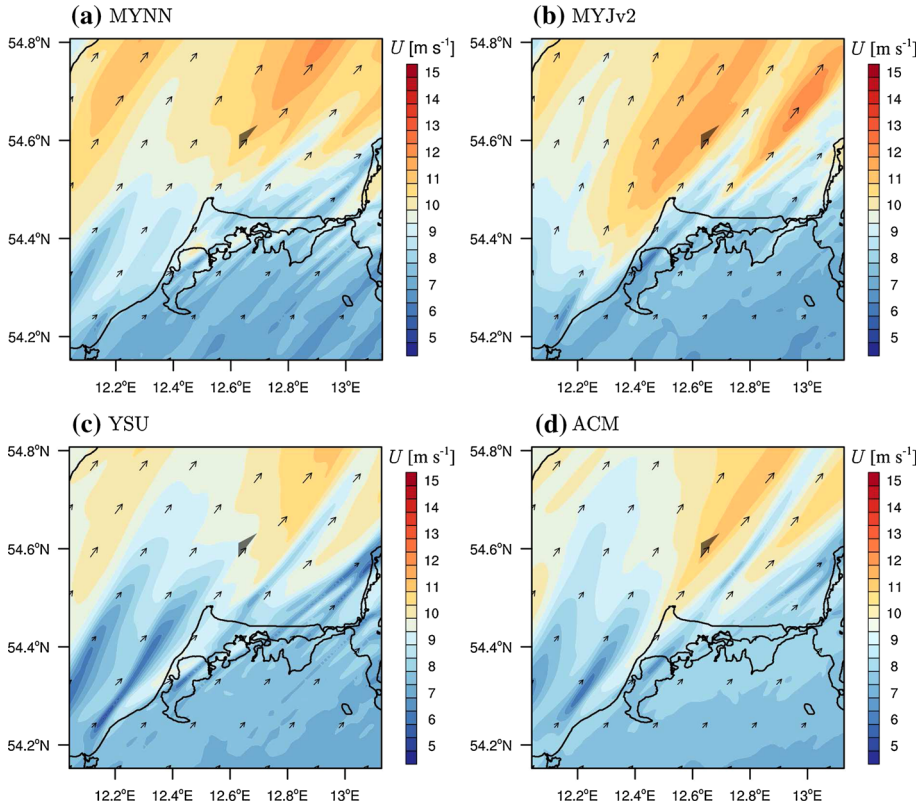


Fig. 17 Hub-height fields ($z = 67$ m) of wind speed for four different PBL schemes [a Mellor–Yamada–Nakanishi–Niino, b Mellor–Yamada–Janjić modified after Foreman and Emeis (2012), c Yonsei University, d Asymmetric Convective Model version 2] obtained from WRF model simulations during stable offshore conditions on 23 July 2012 at 1200 UTC (hourly averages). The grey shaded triangle marks the position and extent of the wind farm

ened afterwards, while the deviations are comparable for all other schemes. Generally the wind speeds tend to be higher in the MYNN and MYJv2 schemes, while they are slightly lower in the ACM and YSU schemes. In summary, it can be stated that there is no large influence of the PBL scheme on the occurrence of roughness-induced streaks of low wind speeds.

References

- Baas P, Bosveld F, Holtslag A (2009) A climatology of nocturnal low-level jets at Cabauw. *J Appl Meteorol* 48:1627–1642. doi:[10.1175/2009JAMC1965.1](https://doi.org/10.1175/2009JAMC1965.1)
- Barthelmie R, Badger J, Pryor S, Hasager CB, Christiansen MB, Jørgensen B (2007) Offshore coastal wind speed gradients: issues for the design and development of large offshore windfarms. *Wind Eng* 31(6):369–382. doi:[10.1260/030952407784079762](https://doi.org/10.1260/030952407784079762)
- Bergström H (2001) Boundary-layer modelling for wind climate estimates. *Wind Eng* 25(5):289–299. doi:[10.1260/030952401760177864](https://doi.org/10.1260/030952401760177864)
- Csanady G (1974) Equilibrium theory of the planetary boundary layer with an inversion lid. *Boundary-Layer Meteorol* 6(1–2):63–79. doi:[10.1007/BF00232477](https://doi.org/10.1007/BF00232477)

- Donlon CJ, Martin M, Stark J, Roberts-Jones J, Fiedler E, Wimmer W (2012) The operational sea surface temperature and sea ice analysis (ostia) system. *Remote Sens Environ* 116:140–158. doi:[10.1016/j.rse.2010.10.017](https://doi.org/10.1016/j.rse.2010.10.017)
- Doran J, Gryning SE (1987) Wind and temperature structure over a land–water–land area. *J Appl Meteorol* 26:973–979. doi:[10.1175/1520-0450\(1987\)026<0973:WATSOA>2.0.CO;2](https://doi.org/10.1175/1520-0450(1987)026<0973:WATSOA>2.0.CO;2)
- Dörenkämper M, Tambke J, Steinfeld G, Heinemann D, Kühn M (2014) Atmospheric impacts on power curves of multi-megawatt offshore wind turbines. *J Phys* 555:012029. doi:[10.1088/1742-6596/555/1/012029](https://doi.org/10.1088/1742-6596/555/1/012029)
- Draxl C, Hahmann AN, Peña A, Giebel G (2014) Evaluating winds and vertical wind shear from weather research and forecasting model forecasts using seven planetary boundary layer schemes. *Wind Energy* 17:39–55. doi:[10.1002/we.1555](https://doi.org/10.1002/we.1555)
- Emeis S (2010) A simple analytical wind park model considering atmospheric stability. *Wind Energy* 13(5):459–469. doi:[10.1002/we.367](https://doi.org/10.1002/we.367)
- EWEA (2013) Deep water—the next step for offshore wind energy. Technical Report. European Wind Energy Association, Brussels, 51 pp
- EWEA (2014) The european offshore wind industry—key trends and statistics 2013. Technical Report. European Wind Energy Association, Brussels, 22 pp
- FINO2 (2007) FINO2 measurement platform—installation protocol. Technical Report. Wind Consult, 152 pp
- Foreman RJ, Emeis S (2012) A method for increasing the turbulent kinetic energy in the Mellor–Yamada–Janjić boundary-layer parametrization. *Boundary-Layer Meteorol.* 145(2):329–349 doi:[10.1007/s10546-012-9227-4](https://doi.org/10.1007/s10546-012-9227-4)
- Foreman RJ, Emeis S, Canadillas B (2015) Half-order stable boundary-layer parametrization without the eddy viscosity approach for use in numerical weather prediction. *Boundary-Layer Meteorol.* 154(2):207–228 doi:[10.1007/s10546-014-9969-4](https://doi.org/10.1007/s10546-014-9969-4)
- Grisogono B, Tjernström M (1996) Thermal mesoscale circulations on the Baltic coast: 2. Perturbation of surface parameters. *J Geophys Res* 101(D14):18999–19012. doi:[10.1029/96JD01207](https://doi.org/10.1029/96JD01207)
- GWEC (2013) Global wind report, annual market update 2013. Technical Report. Global Wind Energy Council, Brussels, 80 pp
- Hansen KS, Barthelmie RJ, Jensen LE, Sommer A (2012) The impact of turbulence intensity and atmospheric stability on power deficits due to wind turbine wakes at Horns Rev wind farm. *Wind Energy* 15:183–196. doi:[10.1002/we.512](https://doi.org/10.1002/we.512)
- Hasager CB, Badger M, Peña A, Larsén XG, Bingöl F (2011) SAR-based wind resource statistics in the Baltic Sea. *Remote Sens* 3(1):117–144. doi:[10.3390/rs3010117](https://doi.org/10.3390/rs3010117)
- Hong SY, Noh Y, Dudhia J (2006) A new vertical diffusion package with an explicit treatment of entrainment processes. *Mon Weather Rev* 134(9):2318–2341. doi:[10.1175/MWR3199.1](https://doi.org/10.1175/MWR3199.1)
- Lange B, Larsen S, Højstrup J, Barthelmie R (2004) Importance of thermal effects and sea surface roughness for offshore wind resource assessment. *J Wind Eng Ind Aerodyn* 92(11):959–988. doi:[10.1016/j.jweia.2004.05.005](https://doi.org/10.1016/j.jweia.2004.05.005)
- Mellor GL, Yamada T (1982) Development of a turbulence closure model for geophysical fluid problems. *Rev Geophys Space Phys* 20(4):851–875. doi:[10.1029/RG020i004p00851](https://doi.org/10.1029/RG020i004p00851)
- Nakanishi M, Niino H (2004) An improved Mellor–Yamada level-3 model with condensation physics: its design and verification. *Boundary-Layer Meteorol* 112:1–31. doi:[10.1023/B:BOUN.0000020164.04146.98](https://doi.org/10.1023/B:BOUN.0000020164.04146.98)
- NCEP (2011) NCEP climate forecast system version 2 (CFSv2) selected hourly time-series products. Technical Report. Environmental Modeling Center/National Centers for Environmental Prediction/National Weather Service/NOAA/U.S. Department of Commerce, Research Data Archive at the National Center for Atmospheric Research, Computational and Information Systems Laboratory, Boulder (updated monthly). <http://rda.ucar.edu/datasets/ds094.1/>
- Peña A, Hahmann A, Hasager C, Bingöl F, Karagali I, Badger J, Badger M, Clausen N (2011) South Baltic wind atlas. Technical Report. Ris-R-1775(EN), Technical University of Denmark, 66 pp
- Pleim JE (2007) A combined local and nonlocal closure model for the atmospheric boundary layer. Part I: Model description and testing. *J Appl Meteorol Clim* 46(9):1383–1395. doi:[10.1175/JAM2534.1](https://doi.org/10.1175/JAM2534.1)
- Pryor S, Barthelmie R (1998) Analysis of the effect of the coastal discontinuity on near-surface flow. *Ann Geophys* 16(7):882–888. doi:[10.1007/s00585-998-0882-3](https://doi.org/10.1007/s00585-998-0882-3)
- Sathe A, Gryning SE, Peña A (2011) Comparison of the atmospheric stability and wind profiles at two wind farm sites over a long marine fetch in the North Sea. *Wind Energy* 14(6):767–780. doi:[10.1002/we.456](https://doi.org/10.1002/we.456)
- Skamarock W, Klemp J, Dudhia J, Gill D, Barker D, Duda M, Huang X, Wang W, Powers J (2008) A description of the advanced research WRF version 3. Technical Report. NCAR/TN475+STR, NCAR—National Center for Atmospheric Research, Boulder, 125 pp. doi:[10.5065/D68S4MVH](https://doi.org/10.5065/D68S4MVH)
- Smedman AS (1991) Occurrence of roll circulations in a shallow boundary layer. *Boundary-Layer Meteorol* 57(4):343–358. doi:[10.1007/BF00120053](https://doi.org/10.1007/BF00120053)

- Smedman AS, Högström U, Bergström H (1996) Low level jets—a decisive factor for off-shore wind energy siting in the Baltic Sea. *Wind Eng* 20(3):137–147
- Smedman AS, Bergström H, Grisogono B (1997) Evolution of stable internal boundary layers over a cold sea. *J Geophys Res* 102(C1):1091–1099. doi:[10.1029/96JC02782](https://doi.org/10.1029/96JC02782)
- Tjernström M, Grisogono B (1996) Thermal mesoscale circulations on the Baltic coast: 1. Numerical case study. *J Geophys Res* 101(D14):18979–18997. doi:[10.1029/96JD01201](https://doi.org/10.1029/96JD01201)
- Tjernström M, Smedman AS (1993) The vertical turbulence structure of the coastal marine atmospheric boundary layer. *J Geophys Res* 98(C3):4809–4826. doi:[10.1029/92JC02610](https://doi.org/10.1029/92JC02610)
- Vincent CL, Larsén XG, Larsen SE, Sørensen P (2013) Cross-spectra over the sea from observations and mesoscale modelling. *Boundary-Layer Meteorol* 146:297–318. doi:[10.1007/s10546-012-9754-1](https://doi.org/10.1007/s10546-012-9754-1)